

# Dynamical theory driven observational analysis of ENSO modes in the equatorial Pacific

Bryan C. Weare<sup>1</sup>

Received: 10 April 2015 / Accepted: 13 November 2015 / Published online: 25 November 2015  
© Springer-Verlag Berlin Heidelberg 2015

**Abstract** The dynamics of tropical Pacific sea surface height changes associated with El Niño/Southern Oscillation (ENSO) have been explored using a melding of a simple dynamical model and maximum covariance analysis (MCA). Two dominant MCA modes, which are degenerate and well correlated at a lag of about 4 months, have a combined time series which is strongly correlated with the Niño3.4 ENSO index. The leading Equatorial Mode shows a strong equatorial signature and is associated with Kelvin wave forcing, Ekman pumping, the wind stress curl, and the Recharge Oscillator hypothesis. The lagging East/West Mode shows a less equatorially trapped east/west pattern of variation and is most associated with zonal wind stress and the Delayed Oscillator hypothesis. The net effect of internal equatorial Rossby waves is dissipative and is not confined to the western boundary. The relevant zonal stress and stress curl fields stretch across the basin. Additional analyses show that both the zonal wind stress and the wind stress curl terms are required for the development of classic ENSO events. Removal of either term gives rise to weaker events, which have properties similar to the central Pacific ENSO events. The seasonal phase-locking of ENSO events is shown to be related to a north to south excursion of wind stress anomalies.

**Keywords** ENSO · Ocean dynamics · Maximum covariance analysis

## 1 Introduction

El Niño/Southern Oscillation (ENSO) is the predominant interannual variability of the global climate system. ENSO is fundamentally a strongly coupled ocean/atmosphere phenomenon in and above the equatorial Pacific Ocean (Neelin 2011; Trenberth 1997; Philander 1990), and is associated with year-long fluctuations throughout much of the globe (Glantz 2001). The outlines of the mechanisms for El Niño were diagnosed from observations in the 1970s, emulated in simple models in the 1980s (Neelin et al. 1998), and at the same time incorporated into full coupled ocean/atmosphere climate and forecast models (Latif et al. 1998).

Our fundamental understanding of ENSO is summarized by Schneider et al. (1995), Neelin et al. (1998), Wang and Fiedler (2006) and Clarke (2008). The current paradigms combine the ocean/atmosphere growth mechanism first introduced by Bjerknes (1969) with additional feedback mechanisms to explain both the initiation and decay of a warm or cold ENSO event. The Bjerknes mechanism states that once a warmer than normal patch of water appears in the central Pacific this anomaly will strengthen through a positive feedback mediated by changes in sea surface temperatures and wind stresses. Clarke (2008) uses models of the equatorially averaged dynamics to describe the Delayed Oscillator (Suarez and Schopf 1988) and the Recharge Oscillator (Jin 1997), the two most important ENSO feedback mechanisms. He describes how for the Delayed Oscillator oceanic equatorial zonal advection, driven by zonal wind stresses, is coupled with Rossby and Kelvin waves to provide time delays. These modify an initial instability leading to the development and decay of an ENSO event. In the Recharge Oscillator variations in the equatorial wind stress curl in the central basin alter the heat storage along

---

✉ Bryan C. Weare  
bcweare@ucdavis.edu

<sup>1</sup> Atmospheric Science Program, Land, Air and Water Resources, University of California, Davis, CA, USA

the equator leading to ENSO events. Intermediate coupled models (e.g. Zebiak and Cane 1987) usually include the influences of both the zonal wind stresses and wind stress curl variations most associated with these feedbacks and sometimes additional processes such as the influence of wave reflection at the western boundary and surface heat flux anomalies.

In recent years there has been a great deal of interest in investigating different flavors of ENSO events (Capotondi et al. 2015; Su et al. 2014; Yu 2012). The most common variations are the classic ENSO events, whose mature phases are centered in the eastern ocean and are sometimes labeled Eastern Pacific (EP) events, and those events which are centered in the central Pacific (CP). Ren and Jin (2011, 2013) provide an excellent description of the nature of these variations, the several indices used to describe them, and mechanisms that may be responsible for the central Pacific events. Several authors (Ren and Jin 2013; Singh and Delcroix 2013; Kug et al. 2009) focus on the relative importance of the heat content variations of the Recharge Oscillator and zonal advection feedback mechanisms, associated with the Delayed Oscillator, in driving the classic ENSO (EP) and central Pacific (CP) events. Additional questions surrounding both types of ENSO events revolve around the role of high latitude variations, the phase locking of most events to the seasonal cycle, and the temporal shifts in the ENSO phenomenon that might be related to climate change.

For more than 40 years observations have been used to display and understand the many interactions between various parameters during ENSO events. Most of these studies have used some combination of correlation, regression and compositing methodologies, utilizing a reference index time series such as Niño3.4. A much smaller number of papers have avoided the use of such indices by utilizing two-field eigenfunction methodologies such as Combined Empirical Orthogonal Functions or canonical correlation analysis (von Storch and Zwiers 1999). Several of these papers (e.g., Wu and Hsieh 2002; Yu et al. 2011) were used to improve statistical forecasts of ENSO. Others such as Weare (2014) and Xu et al. (2014) used these methods to characterize observations and model output. Others (e.g. Luo and Yamagat 2002; Vimont et al. 2003a, b) have explored extratropical teleconnections. However, overall, there has been little work using these methods to better understand the fundamental dynamics of ENSO events.

The goal of this work is to combine theory and observations in order to better integrate the vast research area surrounding ENSO. This study introduces an eigenfunction procedure uniting observations with ocean dynamical theory in order to develop a comprehensive description of the processes involved in the Delayed Oscillator and the Recharge/

Discharge hypotheses. This method loosely follows the forecasting methodologies using canonical correlation analysis (CCA; Barnston and Ropelewski 1992) and Linear Inverse Modeling (LIM; Penland and Magorian 1993). However, in the present case the analysis utilizes a dynamical ocean model framework and puts emphasis on visualizing the latitude-longitude-time relationships between the various terms rather than maximizing forecast skill.

## 2 Data and analysis

The primary data employed for this study are sea surface height (SSH), which is a measure of the average temperature in the upper ocean. The SSH and surface wind stress observations are from the Simple Ocean Data Assimilation (SODA 2.1.6; Carton and Giese 2008) with a horizontal resolution of  $0.5^\circ$  in longitude and  $0.5^\circ$  in latitude for the period 1958-2008. This reanalysis is based on the Parallel Ocean Program model (Smith et al. 1992) with 40 vertical levels. Ocean observations include nearly all available surface observations, satellite surface temperatures, TOGA-TAO (<http://www.pmel.noaa.gov/tao/>) temperatures at depth and satellite altimetry. The atmospheric input is the European Centre for Medium-Range Weather Forecasting ERA-40 reanalysis (Uppala et al. 2005), which is supplemented by the ERA interim analysis (<http://www.ecmwf.int/en/research/climate-reanalysis/era-interim>) for the period after 2001. Also used was the Niño3.4 ENSO sea surface temperature (SST) index, which is commonly used as an EP ENSO index ([http://www.cpc.ncep.noaa.gov/products/analysis\\_monitoring/ensostuff/ensoyears.shtml](http://www.cpc.ncep.noaa.gov/products/analysis_monitoring/ensostuff/ensoyears.shtml)).

The main statistical tool in this study is maximum covariance analysis (MCA; Vimont et al. 2003a, b; von Storch and Zwiers 1999; Bretherton et al. 1992). MCA identifies the patterns of the strongest time covariances between two sets of data. The basic MCA method will be described in order to make clear how the current modification is implemented. The initial step in MCA is the calculation of a covariance matrix  $C$ , derived from the products of time variations at each point in  $S$ , an  $N_s$  point data set, and those in  $Z$ , an  $N_z$  data set, each having  $M$  times.

$$C = SZ^T/M; \quad S = \begin{pmatrix} s_{11} & s_{12} & \cdots & s_{1M} \\ s_{12} & s_{22} & \cdots & \cdot \\ \cdot & \cdot & \cdot & \cdot \\ s_{N1} & \cdot & \cdot & s_{N_s M} \end{pmatrix}; \quad (1)$$

$$Z = \begin{pmatrix} z_{11} & z_{12} & \cdots & z_{1M} \\ z_{12} & z_{22} & \cdots & \cdot \\ \cdot & \cdot & \cdot & \cdot \\ z_{N1} & \cdot & \cdot & z_{N_z M} \end{pmatrix}$$

This matrix is then decomposed into right  $\mathbf{R}$  and left  $\mathbf{L}$  matrices of vectors associated with singular values  $\omega_i$ , such that

$$\mathbf{C} = \mathbf{L} \boldsymbol{\omega} \mathbf{R}^T \tag{2}$$

where  $\boldsymbol{\omega}$  is an ordered diagonal matrix of singular values. The ordering is such that the first left  $\mathbf{L}_1$  and right  $\mathbf{R}_1$  vectors are associated with the largest explained squared covariance between the  $\mathbf{S}$  and  $\mathbf{Z}$  fields and so forth for  $\mathbf{L}_2, \mathbf{L}_3, \dots$ . Associated with these vectors, which are orthogonal in space, are the left  $a_i(t)$  and right  $b_i(t)$  time coefficients defined by inner products such that

$$a_i(t) = \mathbf{L}_i \cdot \mathbf{S}(t); \quad b_i(t) = \mathbf{R}_i \cdot \mathbf{Z}(t) \tag{3}$$

Reconstituted data fields  $\mathbf{S}_i$  and  $\mathbf{Z}_i$ , equivalent to multiple regression estimates, may be determined for each MCA  $i$  by

$$\mathbf{S}_i(t) = a_i(t) \mathbf{L}_i; \quad \mathbf{Z}_i(t) = b_i(t) \mathbf{R}_i \tag{4}$$

The low order  $i$  estimates of  $\mathbf{S}_i$  and  $\mathbf{Z}_i$  are the projections of the original fields that explain the greatest squared covariance.

In order to focus on the oceanic mechanisms of ENSO variability the MCA is combined with a model of large scale ocean dynamics. This model begins with a two layer ocean on the beta plane (Garzoli and Katz 1983) in terms of zonal velocity  $u$ , meridional velocity  $v$ , sea surface height  $SSH$  and wind stress  $\tau$ .

$$\begin{aligned} u_t - fv + g'h_x &= \frac{1}{\rho_0 H_0} \tau^x \\ v_t + fu + g'h_y &= \frac{1}{\rho_0 H_0} \tau^y \end{aligned} \tag{5}$$

$$SSH_t + H_0(u_x + v_y) = 0$$

$f$  is the Coriolis parameter,  $g'$  the reduced gravity,  $H_0$  the depth of the upper layer and  $\rho_0$  the density of that layer. The subscripts identify partial derivatives and superscripts zonal and meridional components. From this one may derive a vorticity equation

$$\begin{aligned} \frac{\partial SSH}{\partial t} = C \frac{\partial SSH}{\partial x} - \left[ \frac{H_0}{f} u_{ty} - \frac{H_0}{f} v_{tx} - \frac{\beta H_0}{f^2} u_t \right] \\ - \vec{k} \cdot \nabla \times \left( \frac{\vec{\tau}}{f \rho_0} \right) \end{aligned} \tag{6}$$

where  $\beta = \frac{\partial f}{\partial y}$  and  $C = \beta g' H_0 / f^2$ , a Rossby wave speed. Garzoli and Katz (1983) find that observations of the tropical Atlantic seasonal cycle show the terms in the bracket are no more than a total of 10 % of the left hand side term. Assuming this also holds for ENSO variations,

$$\frac{\partial SSH}{\partial t} = C \frac{\partial SSH}{\partial x} - \frac{1}{f} \vec{k} \cdot \nabla \times \left( \frac{\vec{\tau}}{\rho_0} \right) - \frac{\beta}{\rho_0 f^2} \tau^x - \varepsilon SSH \tag{7}$$

where the beta term in the curl, which is proportional to the Ekman pumping velocity (Gill 1982), has been explicitly separated out and a dissipation term has been added. The beta term has been expressed this way because it may be shown given  $v = 0$  and ignoring the  $u$  tendency that  $C \frac{\partial SSH}{\partial x} = \frac{\beta}{\rho_0 f^2} \tau^x$ , and thus the equatorial Kelvin wave forcing, is simply proportional to the stress curl.

In the present analysis the left MCA matrix  $\mathbf{S}$  in Eq. 1 is the centered time SSH departure difference for times  $n$  months apart, corresponding to the  $\frac{\partial SSH}{\partial t}$  term. The left matrix  $\mathbf{Z}$  is made up of the combination of the driving terms in Eq. 7,  $-SSH, \frac{\partial SSH}{\partial x}, -\frac{1}{f} \vec{k} \cdot \nabla \times \vec{\tau}$ , and  $-\beta \tau^x / f^2$  for the times of the midpoint of the SSH time differences. Note that the sign of these terms correspond to those in Eq. 7.  $f$  for latitudes less than  $2.5^\circ$  is set to the  $2.5^\circ$  value. In order to emphasize ENSO variations the time difference  $n$  is generally 5 months. The domain of these calculations is  $20^\circ\text{S} - 20^\circ\text{N}$  across the width of the Pacific. The time period is the full record of the available ocean reanalysis, 1958–2008.

As originally suggested by Barnett and Preisendorfer (1987) to reduce the large number of spatial degrees of freedom relative to temporal ones, the MCA inputs are the time coefficients of the dominant ten EOFs of the respective normalized detrended anomaly fields. To create these anomalies long term monthly means for each point are subtracted from the monthly observations. These anomalies are subjected to a 5 month running mean filter. Thereafter the full record trend is removed from each point. Finally, these filtered detrended anomalies are normalized by dividing by the full record standard deviations at each point. This methodology is applied to SSH, the zonal derivative of SSH, the curl of the surface wind stress and the zonal component of the wind stress. The zonal derivative of SSH and the curl of the wind stress are calculated using centered finite differences on a sphere. The first ten EOFs of these fields explain between 38 and 68 % of the total normalized variances.

### 3 Results

The first three MCAs with a 5 month lag in the time difference term explain 58, 37 and 3 % of the total covariance squared, respectively. MCA1 and 2, shown in Fig. 1, dominate the covariability and give a clear view of the mechanisms and processes involved in ENSO development and decay. These two modes are degenerate (von Storch and Zwiers 1999) and thus are associated with a propagating system. The spatial patterns of SSH variations in these modes correspond to the first two EOFs of ENSO-filtered heat content variability (Hasegawa and Hanawa 2003). In order to interpret this figure it must be first observed that the MCA2  $a_2(t)$  time series leads that of MCA1 (Fig. 1k) by

**Fig. 1** Dominant two MCAs of normalized SSH based on Eq. 7. 1 in normalized units. Frames a–j describe the contributions of terms in Eq. 7. Frame k show the time coefficients describing the variations of the patterns. Frame l shows the SSH variations for the Niño3.4 region and the lagged sum of the time coefficients

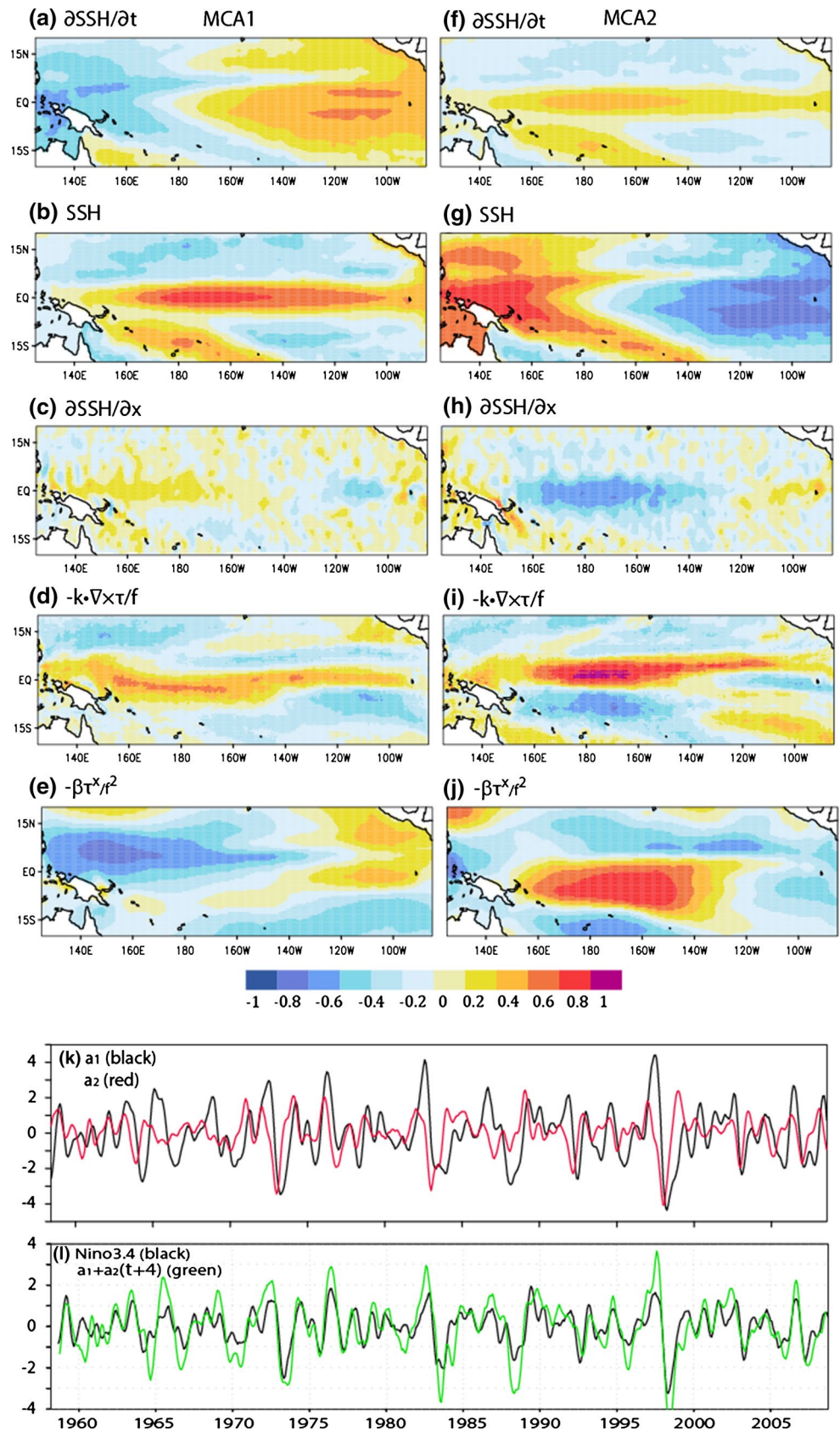




**Table 1** Spatial correlations between terms in the MCA analysis of SSH based on Eq. 7

		20°S–20°N		10°S–10°N		
MCA1	ssh <sub>x</sub>	$-\frac{1}{f}\vec{k} \cdot \nabla \times \vec{\tau}$	$-\beta\tau^x/f^2$	ssh <sub>x</sub>	$-\frac{1}{f}\vec{k} \cdot \nabla \times \vec{\tau}$	$-\beta\tau^x/f^2$
	$\partial\text{SSH}/\partial t$	-0.08	0	0.48	-0.23	0.6
	ssh <sub>x</sub>	-0.24	0.15	0.12	-0.39	-0.1
	$-\frac{1}{f}\vec{k} \cdot \nabla \times \vec{\tau}$		0.04			
MCA2	$\partial\text{SSH}/\partial t$	-0.32	0.22	0.37	-0.46	0.58
	ssh <sub>x</sub>	-0.23	-0.62	-0.25	-0.72	-0.1
	$-\frac{1}{f}\vec{k} \cdot \nabla \times \vec{\tau}$		-0.07			

Correlations with absolute values greater than about 0.1 are significant at the 95 % level, assuming that data at points 5° apart in both latitude and longitude are independent

about 4 months with a correlation of about 0.65. Figure 11 shows the lagged sum  $a(t) = a_1(t + 4) + a_2(t)$  together with the SSH differences spanning 5 months averaged over the Niño3.4 region (170°W–120°W; 5°S–5°N). These two time series have a correlation of 0.81, showing that the MCA has captured much of the ENSO SSH variability over the equatorial Pacific.

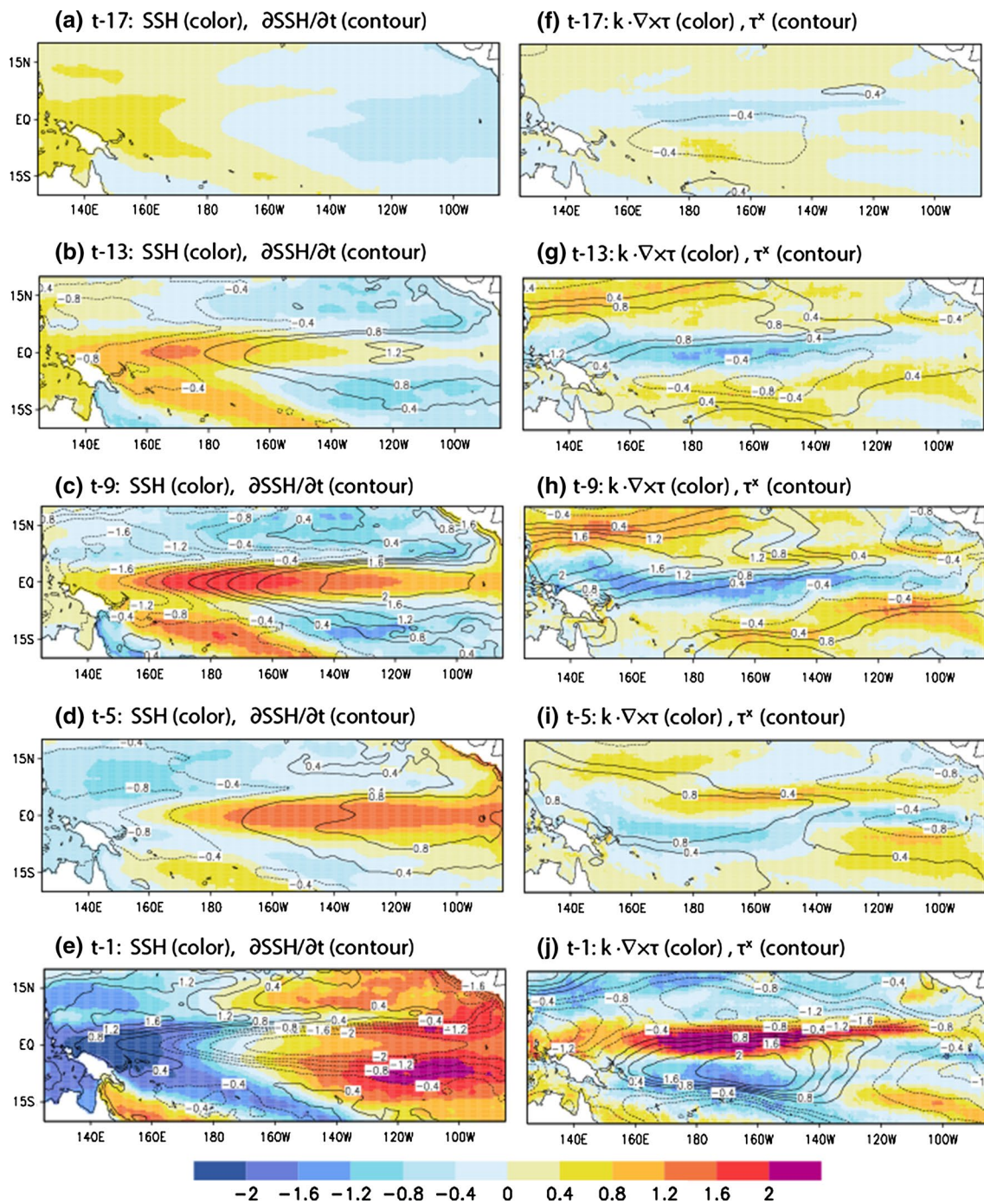
Remembering this lag relation the tendency pattern  $L_2$  of Fig. 1f leads that of  $L_1$  in Fig. 1a. This implies an equatorial heating, which will be called the Equatorial Mode, leads that of a broader east–west heating pattern, which will be called the East/West Mode. After a few months the SSH departures will be dominated by a broad Equatorial maximum and the East/West growth pattern represented by Fig. 1a dominates. These results are consistent with those of Hasegawa and Hanawa (2003) and Meinen and McPhaden (2000), who find that changes in zonally average ocean heat content and warm water volume at the equator lead those in the eastern equatorial Pacific by about 6 months.

Figure 1 and Table 1, showing spatial correlations between various terms in Eq. 7, illustrate a comprehensive picture of ENSO ocean dynamics and lead to a better understanding of the underlying dynamics of ENSO SSH tendency variations. Following the right column in Fig. 1, the earlier Equatorial response occurs when the SSH pattern is in the pre-ENSO state, that is strong negative anomalies in the east and positive anomalies in the west. Table 1 shows that the tendency patterns in both modes are related strongly to the wind stress. However, for the Equatorial Mode this is accompanied by a substantial cancelation in the central and western basin by the damping effects of the Rossby propagation (Fig. 1h). This is the result of westward Rossby propagation bringing low SSH water (Fig. 1g) from the eastern to central and western Pacific Ocean. This cancelation is associated with a Kelvin forcing though a negative wind stress curl term (Fig. 1i), which is significantly related to the tendency (Fig. 1f)

along the equator. This Kelvin Wave driven mode is similar to Ekman pumping along the equator and the meridional Sverdrup transport mechanism described by Masuda et al. (2009), which they state is closely linked to the Recharge Oscillator theory of ENSO. The contributions to the tendency in the Southern Convergence Zone region are unclear.

The East/West Mode follows the Equatorial mode as shown in the left side of Fig. 1. The initial SSH condition for this response is the Equatorial Mode generated positive SSH departures across the equatorial band (Fig. 1b, f). The pattern of the response (Fig. 1a) is similar to that of the negative of the easterly wind stress forcing and not the stress curl term. This pattern is similar to that of the MCA analysis of ENSO peak SST and prior summer zonal wind stress (Vimont et al. 2003a, b). It is this forcing that has been highlighted by most earlier observational studies of ENSO, and is similar to the Bjerknes feedback process, described by Masuda et al. (2009). As shown by Clarke (2008) an eastward wind stress near the equator in the central ocean moves high SSH water from the western basin (Fig. 1g) resulting in a positive anomaly near the dateline (Fig. 1f). There is little cancelation between the influence of Rossby wave propagation (Fig. 1c) and the zonal wind stress (Fig. 1e) as was evident for the Equatorial Mode. The East/West Mode has a curl term that is poorly related to the SSH tendency. Furthermore, the East/West Mode zonal stress anomalies have a distinct east/west pattern, whereas those of the Equatorial Mode response have a largely north/south pattern.

The basin-wide westerly wind stress and wind stress curl patterns in both the Equatorial and East/West Modes are inconsistent with Clarke’s (2014) and Neelin’s (2011) assertion that ENSO is mainly forced by stress changes within 30° of the Dateline. These patterns also suggest, contrary to the summaries of many studies in the ENSO monograph by Clarke (2008), that the relevant wind changes can be associated with longitudinal variation for



**Fig. 2** ENSO EP composites of MCA reconstructed normalized SSH, SSH tendency (a–e), stress curl and westerly stress (f, j) terms from the dominate two SSH MCAs for lags 17, 13, 9, 5 and 1 month

before warm ENSO events. The reconstructions assume that MCA2 leads MCA1 by 4 months

an averaged region a few degrees about the Equator. Strong variations over most of the Tropical Pacific are apparent in Fig. 1 for all fields.

Another way to show these results is to view classic ENSO EP composites of the reconstructions of the lagged sum of MCA1 and 2. These reconstructed maps are defined

by  $M(t) = S_1(t + 4) + S_2(t)$  and the equivalent for the Z fields. These maps are then composited for the moderate and strong warm ENSO events based on the Nino.3.4 index, which peak at 11/63, 11/65, 3/69, 12/72, 1/83, 1/87, 1/92, 11/97, and 12/02. The average  $M(t)$  for the classic ENSO peak times and periods up to 2 years before and after



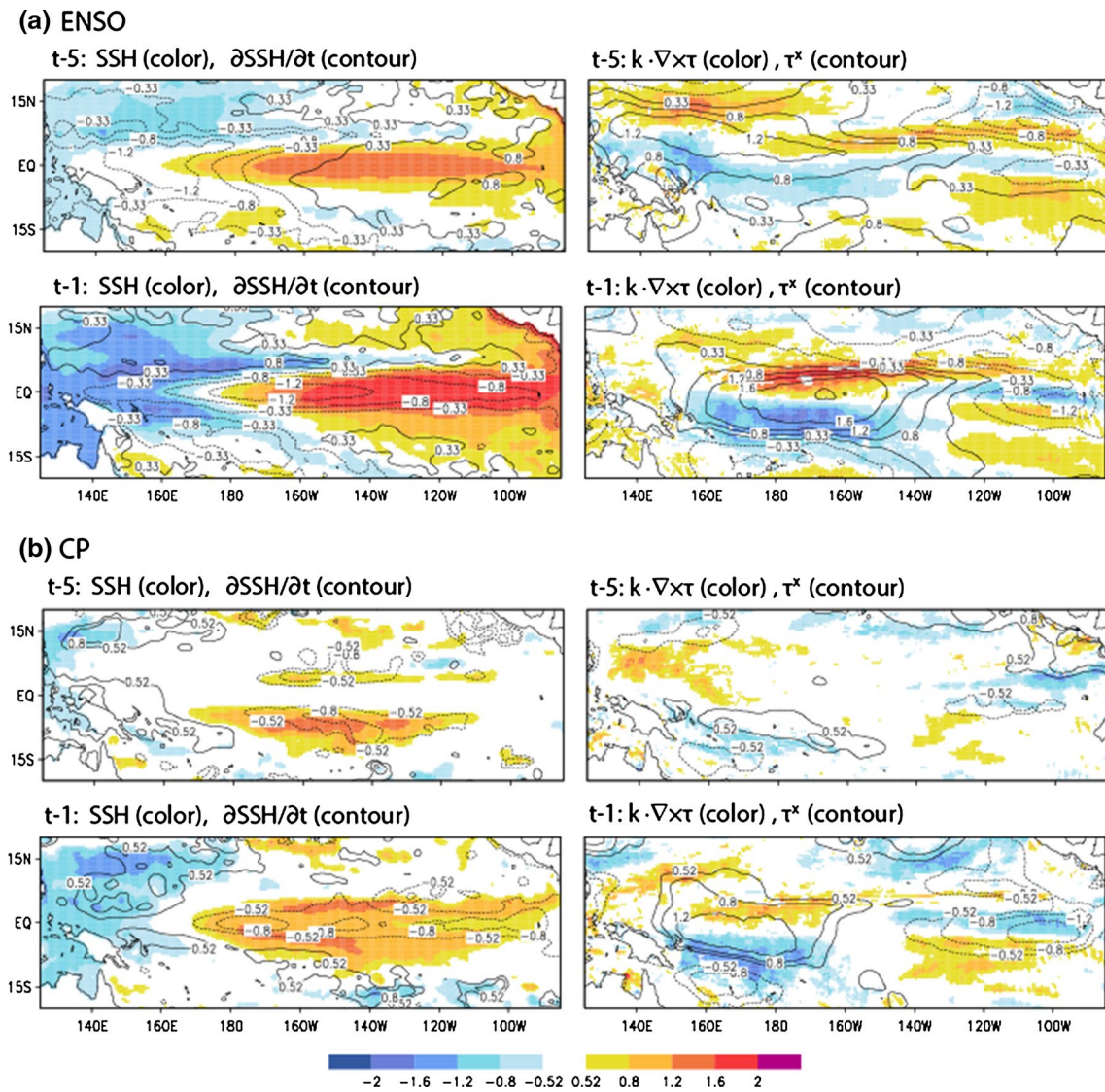


**Fig. 3** ENSO composites of observed normalized SSH, SSH tendency, stress curl and westerly stress terms from normalized observations for lags 5 and 1 month before warm **a** classic ENSO and **b** CP peak events

are calculated. Figure 2 shows the corresponding maps for times from 17 months before the peaks to 1 month before in increments of 4 months for reconstructed SSH,  $\frac{\partial \text{SSH}}{\partial t}$ ,  $\frac{1}{f} \vec{k} \cdot \nabla \times \vec{\tau}$ , and  $\beta \tau^x / f^2$ . 17 months before the warm peak clearly represents the ENSO cold phase with lower SSH in the east and higher in the west. At the same time the zonal stress anomalies are largely negative to the south of the equator. As time progresses to 13 months before the warm ENSO peak there is a positive SSH tendency, whose pattern is related to that of the negative stress curl anomalies along the equator, representing downward Ekman pumping. As time progresses SSH anomalies first propagate eastward along the equator and then poleward up the American coasts. This is accompanied by the eastward propagation of the positive SSH tendency until just before the ENSO

peak at which time the tendency along the equator becomes negative. As this occurs, the negative stress curl anomalies deepen until about 5 months before the peak at which time they become positive. Furthermore, during this time the center of the westerly stress anomalies migrates about  $10^\circ$  from north to south across the equator. This propagation is consistent with the hypothesis of Clarke (2008) describing why ENSO maxima are phase locked to Northern Hemisphere winter. All of these variations are attributable to the lagged interaction between the Equatorial and East/West Modes, shown in Fig. 1.

These composite results may be compared to composites of the direct observations for both the classic ENSO EP events and the CP events. The index for CP events is based on SSH anomaly peaks that occurred in the central

rather than eastern Pacific following Kug et al. (2009). The peak CP months are 1/69, 1/95, 11/02, and 11/04. Figure 3 shows three-month averaged composites (as in Kug et al. 2009) centered on 5 and 1 month preceding either the ENSO or CP peaks. The upper frames of Fig. 3 summarize the classic ENSO EP results and the lower frames the CP events. Looking first at the EP events, there is good agreement between the simple observational composites and those from the dominant MCAs in Fig. 2. In particular the EP peak develops as westerly wind anomalies migrate from north to south as is seen in Fig. 6a–c in Kug et al. (2009). At the same time the wind curl near the equator shifts from negative to positive across most of the basin. These changes support the conclusions of Ren and Jin (2013) that classic ENSO events are driven by a combination of the recharge of equatorial warm water, which is proportional to the wind stress curl changes, and zonal advective feedback, driven by the westerly wind stress changes near the equator. This is consistent with the two modes shown in Fig. 1.

Looking at the lower frames in Fig. 3 one sees that for 1 month preceding the CP maximum the pattern of the anomalies of all four fields are quite similar, although somewhat weaker, to those of the corresponding classic ENSO phase. However, at a lag of 5 months there are relatively few features of the CP composites that are statistically different than zero at the 95 % level. Furthermore, the  $\partial\text{SSH}/\partial t$  field shows a weakening rather than a strengthening of the positive equatorial anomaly seen in the EP composite. This appears to be related to a lack of organized zonal wind and wind curl forcing at this time. The lack of significant variations in the zonal wind is contrary to the composite analysis of Kug et al. (2009) who indicate persistent westerly anomalies at the 925 hPa level in the western equatorial Pacific.

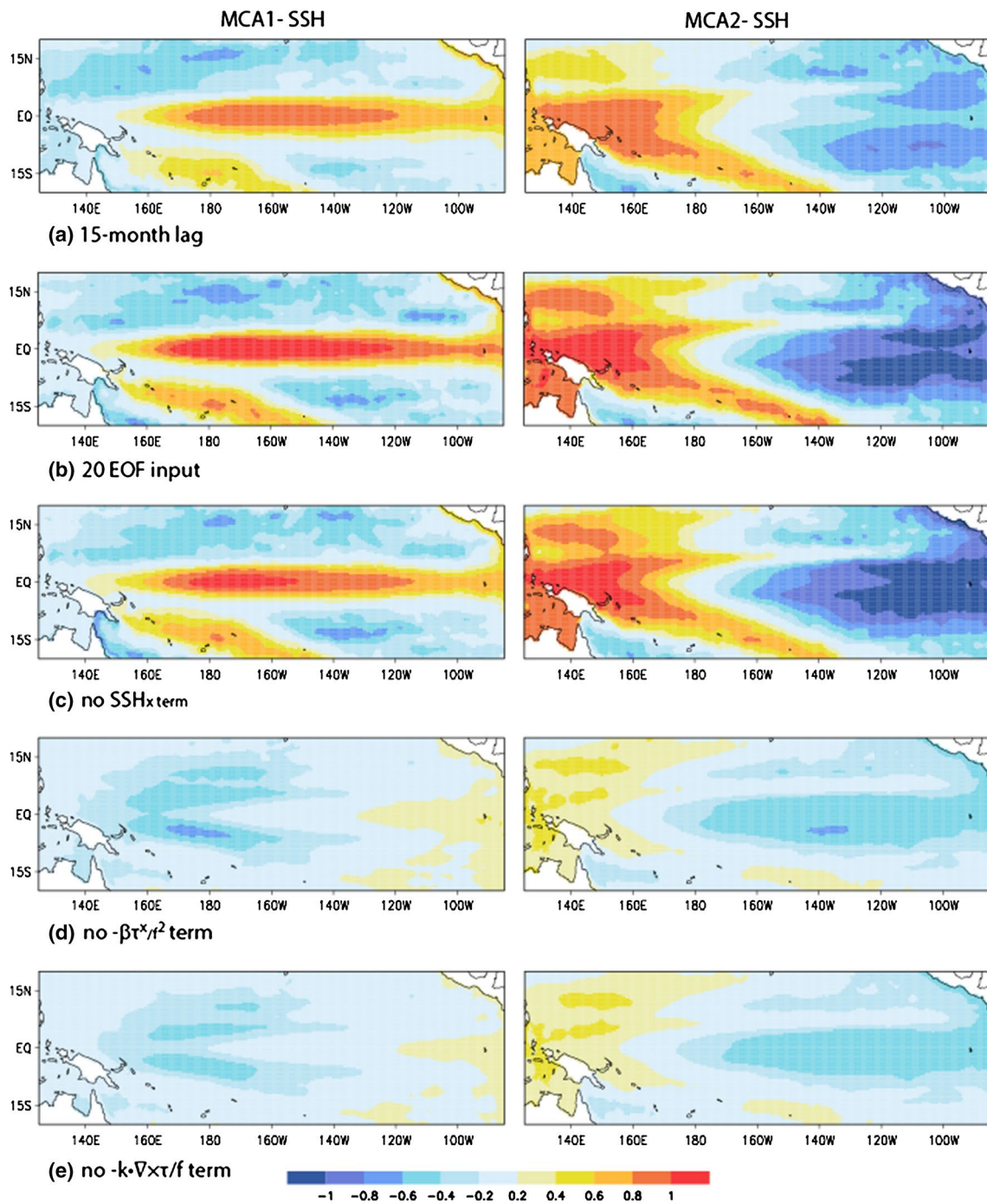
A number of variations of the MCA analysis were carried out to test the robustness of the results and sensitivity to the inclusion of various terms. Figure 4 shows the SSH terms of the first two MCAs for several variations of the methodology. Figure 4a, b show that the results are very similar to those in Fig. 1 for the analysis using a 15 month rather than 5 month lag in the tendency term of Eq. 7 and for the calculations using 20 rather than 10 EOFs of all fields as the inputs. Removing the internal Rossby dissipation term ( $\text{SSH}_x$ ) also does not change the results appreciably (Fig. 4c). Nor does removing the simple SSH dissipation term (not shown). Figure 4 d and e show the dominant SSH terms when the analysis excludes first the zonal wind stress term or the wind stress curl term in Eq. 7. In both of these cases the MCA1 terms are dramatically different from those in Fig. 1, and the MCA2 terms have much weaker west to east contrasts than in the reference analysis. This shows that the full classic ENSO requires organized forcing by both the zonal wind stress and wind stress curl.

Figure 5 further illustrates the influences of removing either the zonal wind stress or stress curl term from Eq. 7 in the MCA analysis. In both cases (Fig. 5a, b) at 1 month prior to the EP maximum ( $t - 1$ ) the SSH departures are weaker and the zone of the maximum departures is shifted westward from that of the full analysis (Fig. 5c). The strength and position of SSH departures for the perturbed analyses are similar to that seen in the CP composites shown in Fig. 3b. At 5 months before the EP maximum the SSH departures for the perturbed analyses are also weaker, but the zones of the maxima are east of those of the full analyses. For both one and 5 month preceding the EP maximum the zonal wind stress and wind stress curl fields are qualitatively very similar to those of the full analysis. This suggests that full blown classic ENSOs require a subtle interaction between the two enabling forcing terms, which may not be present in CP events.

## 4 Discussion

The dynamics of tropical Pacific sea surface height changes associated with ENSO have been clarified using a dynamical ocean model combined with a maximum covariance analysis of observations. The methodology makes no specific assumptions concerning ENSO feedbacks, periodicity or spatial scales, relying only on the basic theory for large scale ocean processes. The analysis identifies two dominant degenerate MCA modes, which explain about 95 % of the covariability and are correlated at a lag of about four months. They have a periodicity of about 35 months and are strongly associated with a common classic ENSO index. The Equatorial Mode shows a strong equatorial signature and is associated with Kelvin wave forcing, wind stress curl, Ekman pumping and the Recharge Oscillator hypothesis. The East/West Mode shows a less equatorially trapped east/west pattern of variation, which is most related to the zonal wind stress and the Delayed Oscillator hypothesis. The net effect of internal equatorial Rossby waves in both modes is dissipative. This emphasizes that the negative feedback in the Delayed Oscillator model is not confined to the “reflection of a Rossby wave front from the western boundary” (Neelin 2011), but is generally true over broad regions and times. The relevant zonal stress and stress curl fields stretch across the basin, rather than being confined to near the dateline. The lagged coupled modes describe the initiation and decay of a full ENSO EP event as described by the Niño3.4 index. Additional analyses show that both the zonal wind stress and the wind stress curl terms are required for the development of classic ENSO events. Removal of either term gives rise to weaker events, which have properties similar to the central Pacific (CP) ENSO events. However, the results are not appreciably changed if





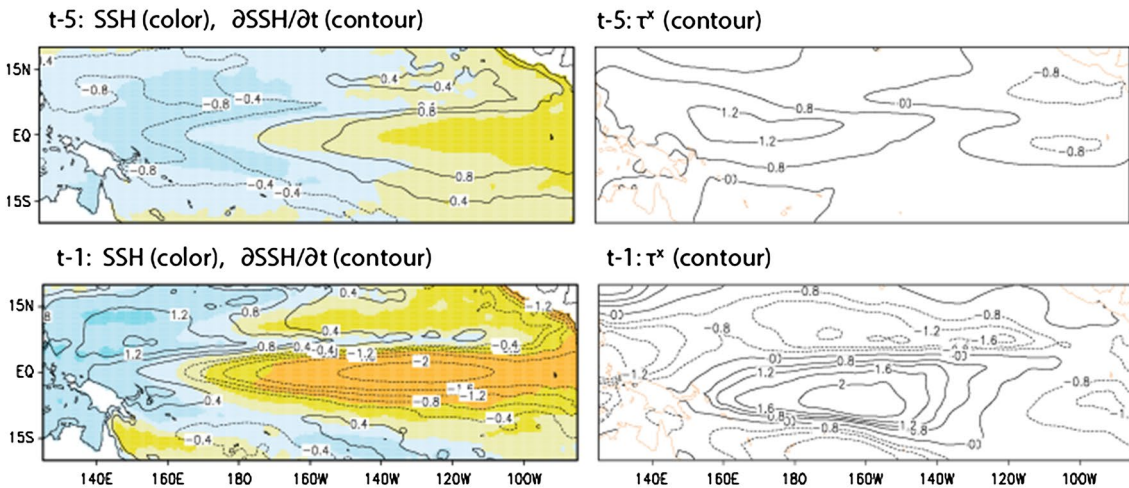
**Fig. 4** SSH term of the dominant two MCAs of normalized SSH based on Eq. 7. 1 in normalized units with modifications: **a** 15 month lag, **b** 20 EOF inputs for each field, **c** no  $SSH_x$  term, **d** no zonal wind stress term, and **e** no wind stress curl term

one removes either the internal Rossby forcing or simple SSH dissipation terms. Furthermore, results suggest that the seasonal phase-locking of ENSO events is related to the north to south migration of wind stress patterns.

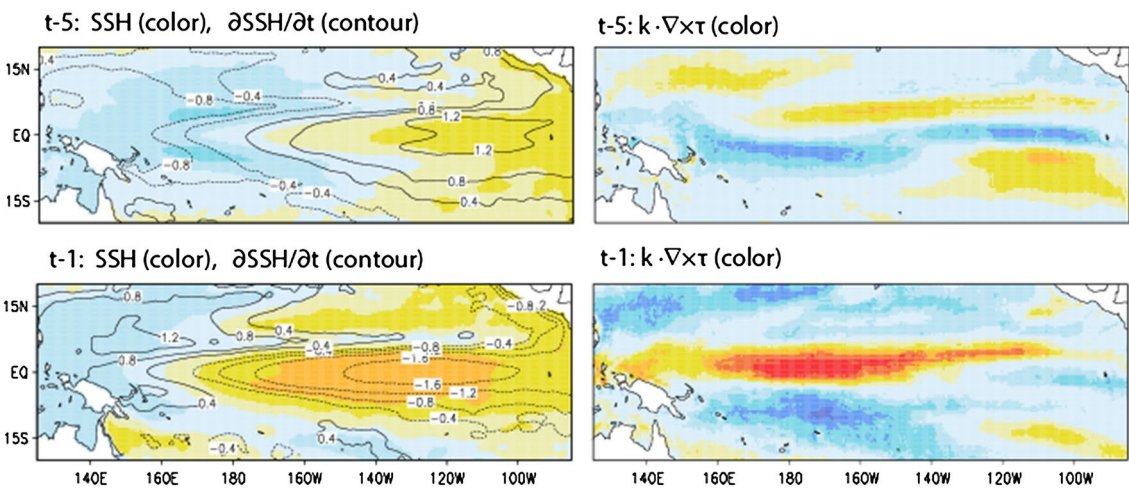
ENSO EP composites of these modes agree well with corresponding ones of the basic observations. Both show the strong interplay between the effects of Ekman pumping,

which is driven by equatorial wind stress curl changes, and equatorial east/west ocean dynamics driven by a north to south migration of zonal wind variations. The corresponding observational composites for central Pacific (CP) events show patterns for the 1 month lag period that are comparable, but weaker and shifted somewhat westward from those of the EP composites. However, the patterns for 5 months

**(a) No  $-k \cdot \nabla \times \tau$  term**



**(b) No  $-\beta \tau^x / f^2$  term**



**(c) All terms**

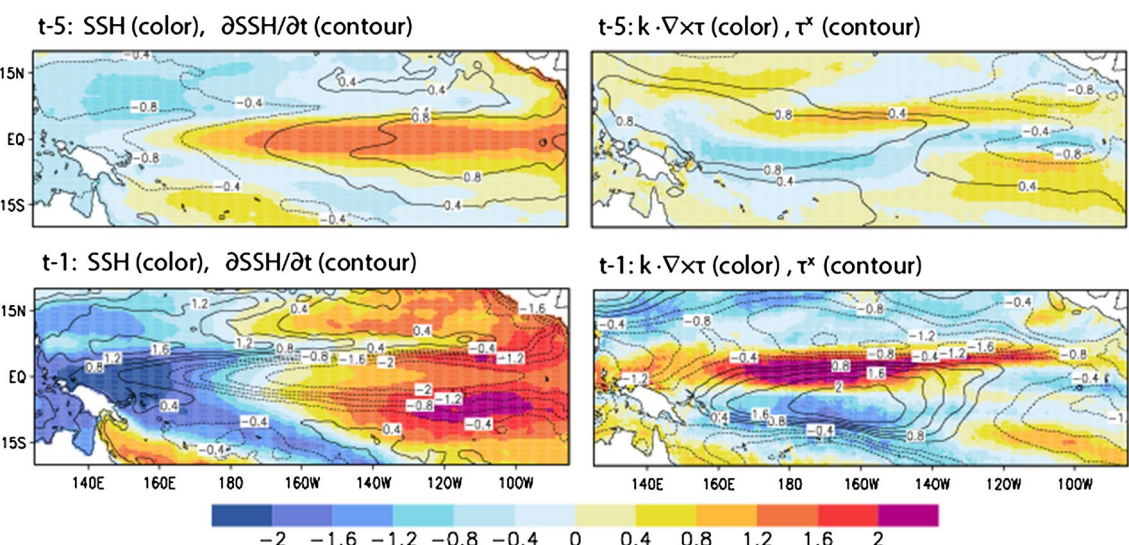


**Fig. 5** ENSO EP composites of MCA reconstructed normalized SSH, SSH tendency, stress curl and westerly stress terms from the events. **a** excluding the zonal stress term, **b** excluding the stress curl term and **c** all terms. The reconstructions assume that MCA2 leads MCA1 by 4 months



before the CP peaks generally show weak equatorial SSH departures and insignificant zonal wind stress and stress curl departure patterns. MCA modes, whose input exclude either the zonal stress or the stress curl terms, show weaker responses that are shifted westward with SSH fields, which are similar to those of the CP SSH composites. This suggests that CP, rather than classic ENSO, events arise when there is a lack of either zonal wind stress or wind stress curl forcing. This is contrary to the results of Kug et al. (2009), who conclude that vertical advection, driven by the stress curl, is the key to classic ENSO events, but that zonal advection, driven by the zonal wind stress, plays a crucial role in CP events.

These results clarify and unify the processes associated with ENSO events that have been suggested by others. Masuda et al. (2009) conclude that both the Sverdrup transport process, similar to the Equatorial Mode, and the westerly stress Bjerknes process, comparable to the East/West Mode, are necessary for a full description of ENSO. The East/West and Equatorial Modes are also equivalent to the first two EOFs of equatorial thermocline depth discussed by Clarke (2014), who relates these modes to both the Recharge and Delayed Oscillator models. Consistent with the current results he found that the East/West Mode is driven by north-to-south westerly wind stress variations and that the Equatorial Mode leads by a few months. Clarke concludes that this north-to-south migration may be the determining factor for the seasonality of ENSO events. Abe et al. (2014) suggest that this may be related to the propagation of off-equatorial Rossby waves associated with variations in the wind stress curl. These in turn are tied to a southward shift in the Intertropical Convergence Zone (ITCZ) in the eastern Pacific, induced by equatorial warming. Thus the ITCZ acts as an atmospheric bridge between equatorial and off-equatorial SSH variations (Hasegawa and Hanawa 2003). Clarke (2014) also suggests that simple forecasts of the Equatorial Mode might be a method to overcome the so-called ‘spring barrier’ for ENSO prediction.

The methodology used here has a number of similarities and differences with statistical forecast models using canonical correlation analysis (CCA; e.g. Wilks 2014; Yu et al. 2011; Wu and Hsieh 2002) or Linear Inverse Modeling (LIM, e.g. Penland and Magorian 1993). In both uses the goal is generally to improve forecast skill, rather than gaining a fuller understanding of the underlying processes. In many applications the input fields are EOF time coefficients, as is done here, and the tendency is set as the time difference over some chosen reference lag, such as the 5 months used here. In LIM the tendency of a field such as Pacific SST is modeled as an autoregressive process with noise. One of the advantages of LIM is that for a Markov process forecasts for other lags are related to those of the

reference lag. The primary limitation of LIM is that it cannot be applied to a more general dynamical model, such as in Eq. 7.

The results suggest additional tools for making statistical forecasts of either warm or cold ENSO events more than 1 year before the warmest or coldest temperatures in the eastern Pacific. Their utility is enhanced by the fact that they depend on defining the SSH tendency only over a 5 month span. However, additional research is necessary to isolate false positives, to identify conditions which conclude as CP events, and to define the factors which are both necessary and sufficient for a useful forecast.

These results do not describe a full ENSO model since the analysis describes only ocean dynamics, utilizing observed stress and stress curl variations, which themselves are responding to the ocean changes. A complete analysis would require an additional equation for the dynamics of the atmosphere near the surface plus a coupling mechanism. Further studies could also explore the role of decadal variability and climate change in ENSO events.

**Acknowledgments** SODA analyses are available at [http://sodaserver.tamu.edu/assim/SODA\\_2.1.6/MONTHLY/](http://sodaserver.tamu.edu/assim/SODA_2.1.6/MONTHLY/). This work was inspired by conversations with Dr. Michael Davey during an extended visit to the Department of Applied Mathematics and Theoretical Physics of Cambridge University.

## References

- Abe H, Tanimoto Y, Hasegawa T, Ebuchi N, Hanawa K (2014) Oceanic Rossby waves induced by the meridional shift of the ITCZ in association with ENSO events. *J Oceanogr* 70:165–174
- Barnett TP, Preisendorfer RW (1987) Origins and levels of monthly and seasonal forecast skill for United States surface air temperature determined by canonical correlation analysis. *Mon Weather Rev* 115:1825–1850
- Barnston AG, Ropelewski CG (1992) Prediction of ENSO episodes using canonical correlation analysis. *J Clim* 5:1316–1345
- Bjerknes J (1969) Atmospheric teleconnections from the equatorial Pacific. *Mon Weather Rev* 97:163–172
- Bretherton CS, Smith C, Wallace JM (1992) An intercomparison of methods for finding coupled patterns in climate data. *J Clim* 5:541–560
- Capotondi A, Wittenberg AT, Newman M, Di Lorenzo E, Yu J-Y, Braconnot P, Cole J, Dewitte B, Giese B, Guiyardi E, Jin F-F, Karnauskas K, Kirtman B, Lee T, Schneider N, Xue Y, Yeh S-W (2015) Understanding ENSO diversity. *Bull Am Meteorol Soc* 96:921–938
- Carton JA, Giese BS (2008) A reanalysis of ocean climate using Simple Ocean Data Assimilation (SODA). *Mon Weather Rev* 136:2999–3017
- Clarke AJ (2008) An introduction to the dynamics of El Niño and the Southern Oscillation. Academic Press, London, p 308
- Clarke AJ (2014) El Niño Physics and El Niño Predictability. *Annu Rev Mar Sci* 6:79–99
- Garzoli SL, Katz EJ (1983) The forced annual reversal of the Atlantic North Equatorial Countercurrent. *J Phys Oceanogr* 13:2082–2090
- Gill AE (1982) Atmosphere–ocean dynamics. Academic Press, New York, p 662



- Glantz MH (2001) *Currents of change*. Cambridge Univ. Press, Cambridge, p 252
- Hasegawa T, Hanawa K (2003) Heat content variability related to ENSO events in the Pacific. *J Phys Oceanogr* 33:407–421
- Jin F-F (1997) An equatorial ocean recharge paradigm for ENSO. Part I: conceptual model. *J Atmos Sci* 45:811–829
- Kug J-S, Jin F-F, An S-I (2009) Two types of El Niño events: cold tongue El Niño and warm pool El Niño. *J Clim* 22:1499–1515
- Latif M, Anderson D, Barnett T, Cane M, Kleeman R, Leetmaa A, O'Brien J, Rosati A, Schneider E (1998) A review of the predictability and prediction of ENSO. *J Geophys Res* 103:14375–14393
- Luo J-J, Yamagat T (2002) Four decadal ocean-atmosphere modes in the North Pacific revealed by various analysis methods. *J Oceanogr* 58:861–876
- Masuda S, Awaji T, Toda T, Shikama Y, Ishikawa Y (2009) Temporal evolution of the equatorial thermocline associated with the 1991–2006 ENSO. *J Geophys Res* 114:C3015–C3024. doi:10.1029/2008JC004953.2009
- Meinen CS, McPhaden MJ (2000) Observations of warm water volume changes in the equatorial Pacific and their relationship to El Niño and La Niña. *J Clim* 13:3551–3559
- Neelin JD (2011) *Climate change and climate modeling*. Cambridge Univ. Press, Cambridge, p 282
- Neelin JD, Battisti DS, Hirst AC, Jin F-F, Wakata Y, Zebiak SE (1998) ENSO theory. *J Geophys Res* 103:14261–14290
- Penland C, Magorian T (1993) Prediction of Niño 3 sea surface temperatures using linear inverse modeling. *J Clim* 6:1067–1076
- Philander G (1990) *El Niño, La Niña, and the southern oscillation*. Academic Press, London, p 289
- Ren H-L, Jin F-F (2011) Niño indices for two types of ENSO. *Geophys Res Lett* 38(L04704):2011. doi:10.1029/2010GL046031
- Ren H-L, Jin F-F (2013) Recharge oscillator mechanisms in two types of ENSO. *J Clim* 26:6506–6523
- Schneider EK, Huang B, Shukla J (1995) Ocean wave dynamics and El Niño. *J Clim* 8:2415–2439
- Singh A, Delcroix T (2013) Eastern and central Pacific ENSO and their relationships to the recharge/discharge oscillator paradigm. *Deep-Sea Res I* 82:32–43
- Smith RD, Dukowicz JK, Malone RC (1992) Parallel ocean general circulation modeling. *Phys D* 60:38–61
- Su J, Li T, Zhang R (2014) The initiation and developing mechanisms of central Pacific El Niños. *J Clim* 27:4473–4485
- Suarez MJ, Schopf PS (1988) A delayed action oscillator for ENSO. *J Atmos Sci* 45:3283–3287
- Trenberth KE (1997) The definition of El Niño. *Bull Am Meteorol Soc* 78:2771–2777
- Uppala SM et al (2005) The ERA-40 re-analysis. *Q J R Meteorol Soc* 131:2961–3012
- Vimont DJ, Battisti DS, Hirst AC (2003a) The seasonal footprinting mechanism in the CSIRO general circulation model. *J Clim* 16:2653–2667
- Vimont DJ, Wallace JM, Battisti DS (2003b) The seasonal footprinting mechanism in the Pacific: implications for ENSO. *J Clim* 16:2668–2675
- von Storch H, Zwier FW (1999) *Statistical analysis in climate research*. Cambridge Univ. Press, Cambridge, p 484
- Wang C, Fiedler PC (2006) ENSO variability and the eastern tropical Pacific: a review. *Prog Oceanogr* 69:239–266
- Weare BC (2014) ENSO modes of the equatorial Pacific Ocean in observations and CMIP5 models. *Clim Dyn* 43:1285–1301
- Wilks DS (2014) Probabilistic canonical correlation analysis forecasts, with application to tropical Pacific sea-surface temperatures. *Int J Climatol* 34:1405–1413
- Wu A, Hsieh WW (2002) Nonlinear canonical analysis of the tropical Pacific wind stress and sea temperature. *Clim Dyn* 19:713–722
- Xu K, Su J, Zhu C (2014) The natural oscillation of two types of ENSO events based on analyses of CMIP5 model control runs. *Adv Atmos Sci* 31:801–813
- Yu J-Y, Chang C-W, Tu Y-Y (2011) Evaluation and improvement of a SVD-based empirical atmospheric model. *Adv Atmos Sci* 28:636–652
- Yu J-Y, Lu M-M, Kim ST (2012) A change in the relationship between tropical central Pacific SST variability and the extratropical atmosphere around 1990. *Environ Res Lett* 7:034025 (6 p)
- Zebiak SE, Cane MA (1987) A model El Niño-southern oscillation. *Mon Weather Rev* 115:2262–2278